NUMERICAL SIMULATION OF THE HOLLOW CATHODE PLASMA USING A PIC-DSMC CODE

Francis T. Crawford and Stephen B. Gabriel

School of Engineering Sciences, University of Southampton, UK

Abstract

The Hollow Cathode (HC) is a device that can be used in a variety of roles within electric propulsion. Interest in micro-thrusters has prompted the need to understand the hollow cathode further, particularly in the case of very small hollow cathodes. Within the context of small hollow cathodes for micro ion thrusters, as well as plume mode cathode thrusters, a computer model has been developed to study the hollow cathode internal plasma flow. The Neutral gas flow through a hollow cathode is typically rarefied, particularly in the case of low mass flow micro-hollow cathodes. The Direct Simulation Monte Carlo (DSMC) method is used to model the neutral flow through the cathode[1]. Implementing a plasma model upon the DSMC is done by modeling the ions as DSMC species and adding electrostatic dynamics via the Particle–in–Cell (PIC) plasma physics method. Both the DSMC and PIC codes are particle based, and very similar. Electrons are currently modeled as particles. The code is compared to a variety of experimental results from research being conducted in parallel.

1 Introduction

Ion thrusters can offer significant propellant mass savings compared to chemical rockets. One major design objective of an ion thruster is the efficient production of ions from some propellant source. Electron bombardment ionization of a gaseous propellant to form a plasma – from which ions are accelerated to produce thrust – is the main process occurring within an ion thruster. The hollow cathode (HC), illustrated in figure 1 is a device that can provide the large current densities required to ionize the propellant in a discharge chamber (the Kaufmann type ion thruster). It is also possible to use HCs as thrusters in their own right [2]. Hollow cathodes are operated by injecting the propellant, usually a heavy inert gas, into the cathode. It is then ionized to produce a plasma. In figure 1, gas is injected from the left and a discharge formed between the cathode and keeper (anode). The cathode is heated to stimulate the thermionic electron emission that will lead to the formation of a plasma. As the discharge develops, other electron emission processes begin to occur.

A computational model, discussed in detail later, has been developed to help understand the processes that occur within ion thrusters, as well as how these processes scale with physical size. So-called "direct simulation" or molecular plasma dynamic models have not previously been used to model the plasma within the hollow cathode of an ion thruster, although both main discharge chamber[3] as well as ion optics[4] and plume[5] models have used direct methods. Hall thruster interior flow has been studied using similar methods[6].

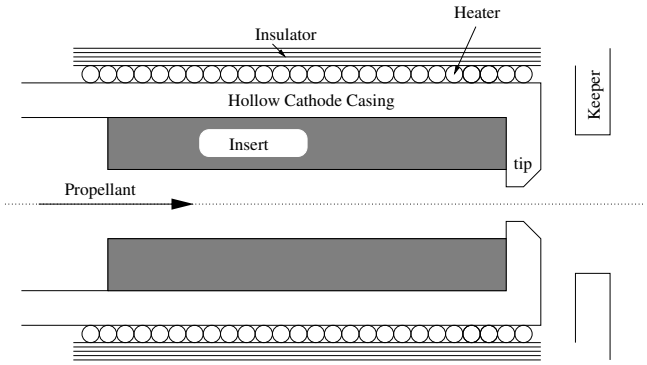

Figure 1: Schematic of a hollow cathode

There are broadly two approaches to the scaling down of ion thrusters, both of which would benefit greatly from a better understanding of the hollow cathode. The issues associated with each are now discussed. Firstly, some have investigated the effect of reducing the discharge chamber dimensions, usually to around the 5 cm range[7]. The use of field emitter arrays (FEA) rather than hollow cathodes has been examined[8], although technical problems remain. Hence, the development of smaller hollow cathodes for the current source is important for such thrusters. The key problem associated with the shrinking of the discharge chamber is a reduced electron residence time within the chamber. Since the ionization probability of an electron entering the chamber is a function of the distance it travels prior to entering the anode(s), the path of the electron is generally lengthened by applying a magnetic field. This causes the electrons to follow a helical path, increasing

the ionization probability. For smaller dimensions, much larger magnetic field strengths are required because the gyration (Lamor) radius of the path is inversely proportional to field magnitude; the mass of these large magnets is prohibitive. Another problem with small discharge chambers is that although ionization is a function of volume, losses depend on chamber surface area; scale reduction increases surface to volume ratio.

Secondly, the approach many are taking is to discard the discharge chamber altogether; the challenges discussed above are perceived too great and several authors[9, 2, 10] feel that operating the hollow cathode in plume mode is the best option. A fully ionized plasma emerges from the cathode and no magnetically confined discharge arrangement is required. It has been suggested[2] that this exhaust could generate reasonable levels thrust and specific impulse due to the presence of very high energy ions. Grid based ion acceleration is also an option. Knowledge of the operating conditions of hollow cathodes in this regime is sparse, and there is research ongoing to understand this mode of operation at the University of Southampton [2].

2 Physical Model

A particle simulation approach has been used for several reasons. Firstly, particle methods have been used successfully for the modeling of several other electric propulsion components and devices[3, 4, 5]. A second motivation for using a particle technique is that the neutral gas dynamics are transitional and rarefied. The Knudsen number, ratio of the mean free path to the characteristic flow dimension, $\mathrm{Kn} = \lambda/L$, is typically used to assess the degree of rarefaction of a gas flow. The DSMC has traditionally been used in the case where the first order Knudsen number approximations inherent in traditional (Navier-Stokes) CFD cause significant error. It will be observed later in the results section that the Knudsen number is unacceptably high for conventional techniques to be used. Finally, it has been observed[11] that the DSMC and PIC techniques combine well in circumstances similar to this one to provide a powerful, accurate modeling technique. Due to disparate constraining parameters, different time steps (τ) and mesh descriptions are used for the PIC and Monte Carlo Collision (MCC) algorithms as well as for different particle types. Further detail regarding the simulation technique follows after a discussion of the underlying numerical methods.

Neutral and ion collisions

Neutral particle collisions are evaluated using the DSMC (NTC) method of Bird[12]. The variable hard sphere collision model is used, such that the total collision cross section is

$$\sigma_T = \pi d_{ref}^2 \left(\frac{2kT_{ref}}{m_r c_r^2} \right)^{\omega - \frac{1}{2}} \Gamma\left(\frac{5}{2} - \omega \right)^{\frac{1}{2}}, \tag{1}$$

where, for a collision between molecules of mass m_a and m_b, $m_r = m_a m_b/(m_a + m_b)$. d_{ref} is the molecular diameter at reference temperature T_{ref}, ω is the viscosity-temperature power law index and c_r is the relative speed between a and b. Parameters for standard ion thruster propellants are $d_{ref} = 4.17 \times 10^{-10}$ m, $\omega = 0.81$ for Argon and $d_{ref} = 5.74 \times 10^{-10}$ m, $\omega = 0.85$ for Xenon[12]. Since only a single inert (monatomic) gas flow is considered, collision models for molecules consisting of more than one atom are not required. Currently, ions are considered as another DSMC species and included in the collision procedures – charge exchange collisions are not included at this stage, but will be later.

Ionization and recombination collisions

Often, hybrid models are in which electrons are modeled as a continuous fluid, while neutrals and ions are modeled as particles. The model presented here currently models electrons as particles. This allows ionization and recombination collisions to be computed explicitly using the methods of Nanbu[11]: the so-called Monte Carlo Collision (MCC) method. In fact, the DSMC can be considered a subset of the MCC technique, albeit highly optimized for molecule-molecule collisions. Electron collisions with neutrals are evaluated using Nanbu's constant τ method. Several collision phenomena need to be modeled: ionization, momentum transfer and excitation. There may be many different levels of excitation. First, all possible collision processes for which data are available are enumerated and collision cross section data σ_k for each process stored in a set of arrays. Then, the probability of the kth collision event occurring in time Δt is $P_k = n_g c_e \sigma_k \Delta t$, where c_e is the electron speed and n_g the neutral gas density. An advantage Nanbu's method is that both the collision event and its success probability can be evaluated using single random number. The electron density may be high enough to warrant the inclusion of couloub collisions[13], however such collisions are not included at this stage.

Plasmadynamics

The particle-in-cell (PIC) plasma physics model of Birdsall and Langdon[14] is used to model the transport properties of charged particles. In the interests of computational simplicity, the electrostatic PIC algorithm is used. Hence, the motion of the jth charged superparticle proceeds as

$$\frac{d\mathbf{v}_j}{dt} = \frac{q_j}{m_j}\left(\mathbf{E} + \mathbf{v}_j \times \mathbf{B}\right), \tag{2}$$

where $\mathbf{v}$ is the particle velcocity vector, q charge, m mass, $\mathbf{E}$ electric field and $\mathbf{B}$ magnetic field. The electrostatic approximation implies that $\mathbf{B}$ is constant. This means that Maxwell's equations reduce so that the electric field can by found using $\mathbf{E} = -\nabla\phi$. The electric potential is obtained from Poisson's equation, expressed here in axially symmetric cylindrical co-ordinates as it is used in the model,

$$\frac{\partial^2\phi}{\partial r^2} + \frac{1}{r}\frac{\partial\phi}{\partial r} + \frac{\partial^2\phi}{\partial z^2} = \frac{\rho_C}{\varepsilon_0} \tag{3}$$

ρ_C is the charge density obtained using $\rho_C = e(n_i - n_e)$ where e is the elementary charge and n_e, n_i the electron and ion number densities respectively. Detail regarding the implementation of the solution of this equation is contained later. PIC field matricies use a different mesh to the that used for the MCC algorithms. No high order particle mesh interpolation or smoothing is used.

3 Computational model

Details regarding the implementation of the algorithms discussed above follow. For the most part, standard procedures suggested by Bird, Nanbu and Birdsall for the implementation of DSMC,MCC and PIC codes are followed: there are no major departures from the standard techniques.

MCC/DSMC implementation

The domain is divided into cells and sub cells of varying radial and axial size. Within the sub cells, populations of computational molecules are stored using an optimized linked list structure. The domain is decomposed axially into n sections of cells that are distributed accross n compute nodes. Radial weighting factors have not been used as suggested for axially symmetric flows[12]. While the use of such weighting factor systems increases computational efficiency, Bird's method has been found to be stable only for flows in which the stream velocity is directed away from the axis. It will be seen in the results section that HC interior flow always involves some degree of negative radial stream velocity near the cathode tip (the minimum area section). The problem of varying radial sample sizes on an orthogonal grid is solved by using a grid where the cell volume is constant with varying radial position. Validation of the DSMC code has been performed by comparison with some standard cases, both non hollow cathode DSMC tests[12] and by empirical comparison to a previous hollow cathode model[15]. Confidence in a particular set of results is increased by running the same physical parameters with different computational parameters. This establishes stability limits for factors such as mesh size, τ and superparticle ratio (FN).

PIC implementation

The PIC code is constructed on top of the DSMC code. This means that the particles' movement, storage and data sampling is inherited from the DSMC/MCC model. The only major addition is the solution of the field equations. Poisson's equation (3) is expressed in finite-difference form on an orthogonal mesh that is derived from the DSMC mesh. While the PIC mesh is constructed from the user-defined DSMC mesh, neither the cell density nor boundary structure are the same. The problem is expressed in linear algebra form ($\mathbf{Ax} = \mathbf{b}$) and solved in parallel. Boundary conditions are applied so that the only boundary that is implicit (Neumann) is the central axis. This means that the problem is not singular and does not require the extra complexity of a singular value decomposition solution.

Parallel implementation

The simulation domain is decomposed axially into segments of cells. Each node of a parallel computer completes all computation on all particles contained in its segment. At the end of each move phase, particles that have moved out of a node's domain are sent to the correct node or removed. On each electron time step, τ_e, the field equations are solved in parallel using the PETSc parallel library using fast implicit solution techniques such as Conjugate Gradient variants. Exactly which solution method used depends on the number of nodes

used. The parallelization used the MPI standard. For the case of distributed (cluster) parallel computers, the code achieves very good scalability and parallel performance for the DSMC/MCC algorithm even on low bandwidth, high latency ethernet interconnect. Performance deteriorates with the inclusion of the PIC code unless high bandwidth communication interconnect can be used; solution of the sparse matrix problem requires much greater communication performance compared to this implementation of the parallel DSMC/MCC method. In fact, were the resources available, the solution of the field equation(s) would be best carried out on a shared memory architecture.

4 Results

The results now follow in two sections. First, the neutral gas flow using the DSMC is examined and discussed. These constitute similar, but enhanced sets to those found in [1]. Secondly, using the first set of results as an initial condition, initial findings using the full PIC-MCC-DSMC model are presented. Parameters now described for the neutral flow are retained for the plasma discharge. The hollow cathode considered for both sets of results that follow is that of the UK T6 ion thruster. This configuration consists of an insert section with radius 1 mm, length 20 mm, a 0.7 mm radius tip and a 2 mm radius keeper located 2.5 mm downstream of the tip. The cathode is 'closed' – no gas or plasma can escape between the cathode body and the keeper. The geometry can be seen in any of the contour plots that follow in the results section. It should be noted that the aspect ratio of the simulation domain is $\sim$9, this meaning that the following plots use an artificially large r scale for clarity. The tip is modeled as square (no bevel) for these results. Although the code provides the ability to use conic sections, it has been found that for the neutral gas flow, there is only a small difference between the beveled and unbeveled cases. Comparison has not yet been made regarding the influence of the bevel on the plasma discharge.

Neutral gas flow boundary conditions and parameters

Hollow cathodes operate in the temperature range 1300° K (during start-up) to 3000° K (during operation). For start-up, the cathode is heated (see figure 1) to at least 1000 K. At greater temperatures, a significant fraction of the low work function compounds (BaO, CaO and Al_2O_3) impregnated into the insert begin to vaporize and are lost.

All but two of the walls that make up the geometry are assumed to be isothermal and diffusely reflecting with full thermal accommodation. One exception is the cylindrical 'wall' that exists between the keeper and the cathode casing. If this wall is included as being specularly reflecting, we can simulate the case of a 'closed cathode' configuration; gas cannot escape between the cathode body and keeper, only downstream of the keeper. The effect of such a specularly reflecting wall is that the gas conditions are mirrored: the mass flux through the wall is zero. For these results, the closed keeper configuration is used. In a similar manner, the upstream boundary is specularly reflecting. Using this method, we can explicitly specify the mass flow rate as a parameter. This is very useful for experimental comparison, where inflow rate is often measured. In the results presented here, the space between the keeper and cathode is non–reflecting, an 'open keeper'.

The keeper temperature is very difficult to quantify. The keeper is situated only a few millimeters from the cathode tip, which is often observed glowing during and after operation. The keeper has never been seen to glow (for this configuration). There is however complete thermal insulation between keeper and cathode; the only transfer of energy from cathode to keeper is via the gas and radiation. In addition, the gas is very cold upon reaching the keeper — it has passed through a normal shock experiencing a temperature drop of more than 300° K. Clearly, the thermal environment surrounding the keeper is complex. Methods available to enhance the thermal modeling of this region are discussed once it is shown how an isothermal keeper at 600° K affects the gas flow.

A constant mass flow rate is applied by injecting particles through the upstream boundary. The temperature of the entering upstream gas is set at 400° K. Application of downstream pressure chamber conditions has been tried, but as would have been expected, any chamber effect has no significant effect on any of the flow. This is because the flow is invariably choked and the Mach number often hypersonic on the downstream boundary; vacuum chamber pressure information does not propagate upstream at all.

The DSMC parameters are set according to the recommendations of Bird[12]. The cell size is manipulated such that the dimensions are always less than 1/3 the mean free path. The time step is set so that τ_n is smaller collision time. Densities of the order 10^{23} m^{-3} exist within the insert section, so that for the gases under consideration (Ar, Kr and Xe) at the temperatures expected, the mean collision rate is $\sim 10^7$ s^{-1}. Hence, typical time steps are in the 10^{-8} second range. During the process of self-validation, τ_n as low as 10^{-10} s have been shown to give identical results to those at 10^{-8} s. The flow tends to converge to a steady state from an empty vacuum start in around 0.3 s real (physical) time. Typically, up-wards of 1.2s real time is modeled in 3-4 hours compute time, with data sampling occurring half way through a run. 1.2 s real time at 10^{-8} s Δt

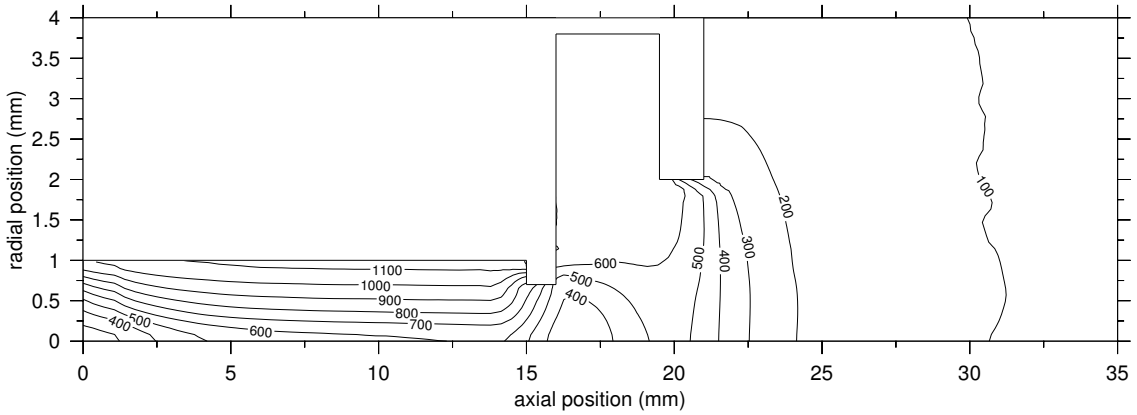

Figure 2: Contours of constant temperature, intervals of 100° K, neutral gas flow of Xenon at 2 mg s^{-1}.

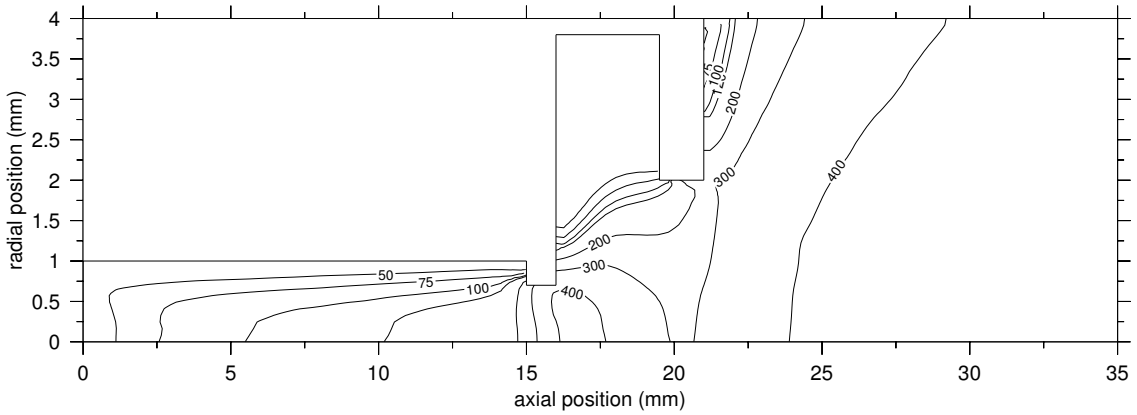

Figure 3: Contours of constant axial stream velocity

corresponds to 120 million time steps. FN, the ratio of real particles to super-particles is set implicitly during runtime and adjusted dynamically. FN is generally around 10^{10}. Depending on the mesh density, which has been tried for cell sizes much smaller than $\lambda/3$, the number of computational particles used ranges from 0.3 to over 1 million computational particles. Mass flow rate and pressure histories are used to judge convergence. It has been found that examining downstream mass flow rate alone is not a sufficient indicator of a steady flow: the flow rate can be constant while transient phenomena are still occurring in the flow. This is particularly the case within the shock waves. If sampling is begun too early, transient (non-equilibrium) pressure profiles can result.

Neutral gas flow results

Examined as a whole, the flow through the hollow cathode geometry is that of a choked nozzle. Subsonic behavior precedes a minimum area point (the tip) where normal, sonic shock wave is present. After the shock, the gas expands further, and leaves the domain at high Mach number. Figure 2 shows temperature contours. Both the temperature boundary layer (Poiseuille flow) and two normal shocks can clearly be seen. Figure 3 shows contours of constant axial stream velocity. The incomplete formation of parabolic radial velocity profile as the flow progresses can be observed. Figure 4 shows Mach number, here the sonic point at the nozzle throat can be seen, followed by a small decelerating normal shock. Further analysis of the detailed features of the flow is divided into two sections: upstream and downstream of the tip, the subsonic and supersonic regions respectively.

Upstream of the tip, the results indicate that the flow is a laminar subsonic Poiseuille flow that is not fully developed. That the flow is laminar is expected: given a mean density in this region of 0.02 kg m^{-3}, on-axis (free) stream velocity ranging between 50 and 200 m s^{-1}, a diameter of 2 mm and viscosity $\mu(\mathrm{Xe}) = 2.107 \times 10^{-5}$ N s m^{-2}, the Reynolds number, Re, is approximately 200. For a *fully developed* Poiseuille flow the onset of turbulent characteristics occur at Re $\sim$ 2000. The DSMC sampling characteristics empirically verify the assessment that the flow is laminar: extensive sampling is not required to eliminate non-equilibrium turbulent effects. Examining the plot of axial stream velocity (fig. 3), it is clear that the flow is not developed. The radial spacing of the velocity contours show a region of constant stream velocity near the centerline; in a fully developed Poiseuille flow the velocity profile is parabolic. The flow behavior observed on the upstream boundary is very similar to expected results for pipe flow. Although the characteristics of Poiseuille flows are archetypal in this case, it is necessary to explicitly state the similarities between accepted fluid dynamic knowledge and the

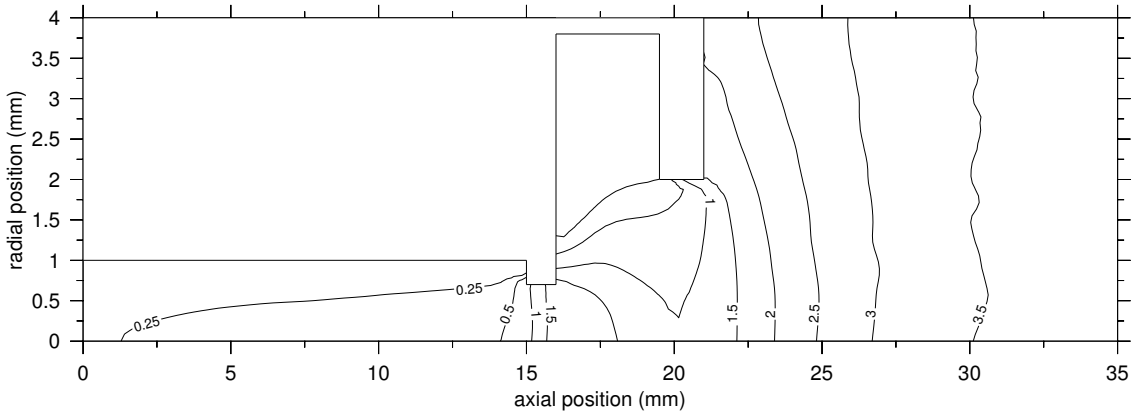

Figure 4: Contours of constant Mach number at intervals of 0.5, and at 0.25

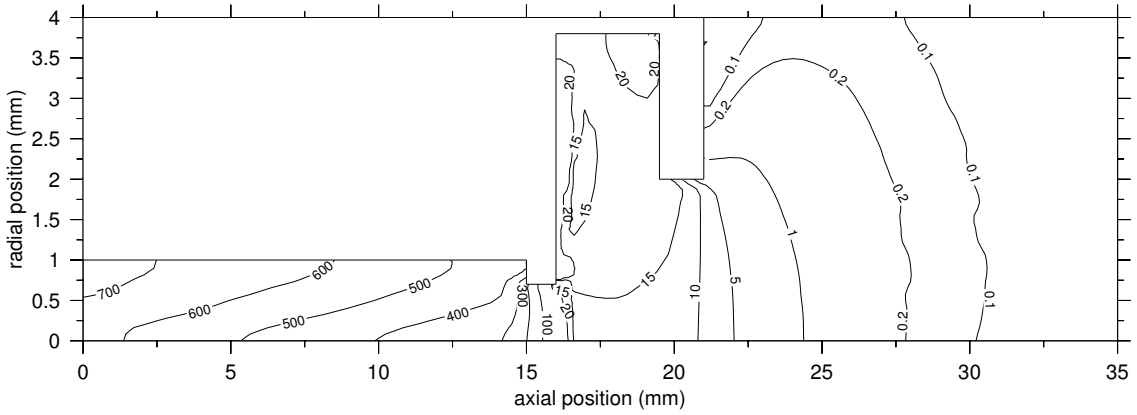

Figure 5: Isobars, note non-linear scaling

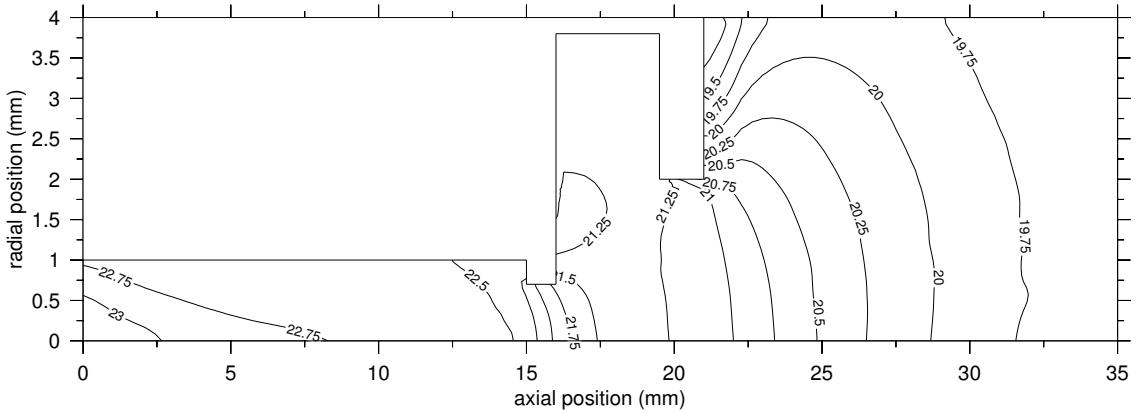

Figure 6: Contours of number density (contour labels 10^x m^{-3}

performance of the DSMC. As will be seen, the DSMC model is operating in a nearly continuum flow regime upstream of the tip. It is important to emphasize that the DSMC is reproducing traditional (continuum) fluid dynamics correctly, while also demonstrating the more spectacular rarefied supersonic flow downstream. The sonic point at the tip involves an acceleration from 200 to 400 m s^{-1} in the space of 1 mm. During the shock, the temperature drops by around 300° K. Hence, the Mach number (fig. 4)rises to above 1.5.

Downstream of the tip, the gas is heated by the warm gas caught in the section between keeper and cathode body re-entering the flow. In this region the flow actually slows and the Mach number drops slightly. Further downstream, adjacent to the keeper, the flow undergoes another normal shock. This shock, attached to the keeper, involves a temperature change of around 200° K with a thickness of ~ 2.5 mm. The gas pressure (fig. 5) drops by about 15 Pa during this shock to 1 Pa before falling away toward the vacuum boundary. Notice that the second shock is much wider and less well defined compared to the first. Although the two shocks are different for several reasons, one predominant reason is the degree of rarefaction present this far downstream. Calculations of Knudsen number based on $L = 2$ mm show that the flow is transitional ($0.1 < \mathrm{Kn} < 1$) within the insert region. During the sonic shock, the Knudsen number rises to around 5. This indicates that the gas has become rarefied. Toward the downstream boundary, Kn$\rightarrow \infty$ as would be expected for an expansion to

vacuum.

The presence of three distinct flow regions – transitional, rarefied and free molecular – within such a small space is of great interest. As the results section proceeds to examine some initial results obtained by including a plasma simulation, it is worth bearing in mind the analysis of the gas dynamics. It is reasonable to suggest that the startup and initial evolution of the plasma discharge will be heavily influenced by these three distinct gas regions. Of course, once a plasma has developed to a reasonable density, then the plasma dynamics of the problem would be expected to have a greater influence on the overall fluid mechanics than the neutral gas dynamics.

Plasma discharge boundary conditions and parameters

The initial results presented here use a computational model built directly upon that used for the above results. The plasma model is in its infancy compared to the neutral model, and we cannot currently have the same confidence in the following results as we have for the neutral gas analysis. The collision cross section data used for Xe in the MCC code is that of Pack and Phelps[16], used by Nanbu in MCC codes previously[13].

All of the surfaces have constant voltage (Dirichlet boundary condition in solution of Poisson equation). The cathode is fixed at 0 V, the keeper at 18 V, mathematically representing Dirichlet boundary conditions to Poisson's equation; all other boundaries use Neumann boundary conditions. Cathodes of this geometry at 1 mgs^{-1} typically exhibit breakdown at around 15 V. That the simulation proceeds to generate plasma breakdown at similar keeper voltages to those observed experimentally provides some empirical validation for the PIC algorithm. At startup, there are zero charged particles in the simulation; no initial distribution is applied. During the simulation, the only applied particle flux (in addition to the continuing neutral flow) is that of electrons leaving the cathode surfaces initially via thermionic emission. This boundary condition is implemented using the Richardson-Dushmann equation: the current density for an element of wall at temperature T_C is

$$j = \frac{4\pi m_e e k^2 T_C^2}{h^3} \exp\left(\frac{-e\phi_w^{eff}}{kT_C}\right), \tag{4}$$

where $\phi_w^{eff} = \phi_w - \sqrt{eE_C/(4\pi\varepsilon_0)}$ is the effective surface work function. In this way, the work function of a wall, ϕ_w is modified by the local electric field strength E_C to model field-assisted electron emission. E_C is simply taken directly from the most recent PIC field solution as the local field magnitude for a given wall cell. The electron work function of tungsten (the cathode body), ϕ_w, used is 4.55 eV. The exact work function of the insert is unknown, as it is impregnated with compounds help to decrease it. A value for the insert ϕ_w of 3.6 eV is used, although even this may be too high. It is possible that field emission contributes a large proportion of the total current extracted from hollow cathodes. Computational electrons are injected at a rate based on the calculated j at energy selected from a Maxwellian distribution based on wall temperature. For this geometry (emission occurring for a 7mm long section of the insert, plus all other cathode surfaces), this implies an average emission current of 0.81 A. The cathode body is set to an artificially high temperature (1950K) to generate a large thermionic current. In reality, as the heater of a hollow cathode raises the temperature, so the current will rise (in a non-linear fashion; see eq. 4). The luxury of modelling gradual temperature changes is not available, so to avoid a 'wall' of current generated by the sudden switching on of current in the simulation, the emitted current is ramped up linearly over a period of 3 μs. The choice of this time period is made to correspond to observations regarding the timescale of the breakdown[17]. This avoids unrealistic electron waves and mechanics that can occur with sudden changes in current. Anode boundaries absorb electrons and diffusely reflect ions as if they were neutral particles. It is anticipated that more realistic wall interactions, i.e. secondary electron emission, will be included soon.

Ions are introduced into the simulation implicitly via ionizing collisions between high energy electrons and the existing neutral gas flow. Clearly, during startup, the neutral particle density will be many orders of magnitude greater than the electron density. To ensure the PIC algorithm charge density mesh receives a smooth distribution, differing super-particle ratios are used: FN_n, FN_e and FN_i[13]. The ion super particle ratio, FN_i is started very low ($< 10^5$) and adjusted as the plasma develops. Time steps used are $\tau_e = 10^{-11}$ s, $\tau_i = \tau_n = 10^{-10}$ s. Unlike the neutral gas results, time step independence has not been established, although it is anticipated that 10^{-11} s will be shown to be a conservative value. It has been found that solving the field equations on a timestep much larger that 3×10^{-10} introduces un-physical electron behaviour[14]. Plots of electron particle tracks clearly reproduce correct electron motion even for electrons at > 30 eV near the keeper. Examination of such plots is a good way to judge the realism and stability of PIC simulations[14]. The use of such tracks is used as empirical proof that the electron motion is natural rather than driven by the grid and or timestep[14]. The PIC mesh used falls broadly within the tolerance of $1/3$ Debye length[14], although there are some regions that require a finer mesh. Due to constraints in the size of the field solution, the domain size is reduced by shortening it from both ends compared to the previous neutral gas results. Charged particles experience an identical upstream condition to neutrals: the specularly reflecting boundary described previously.

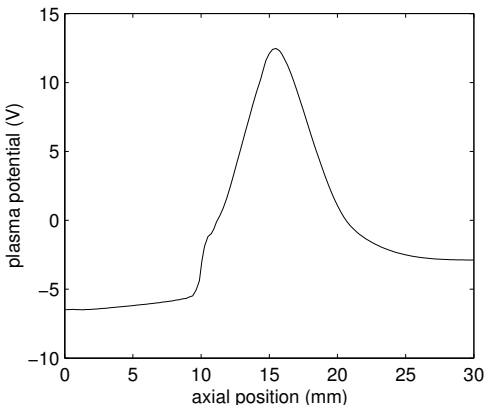

Figure 7: Axial potential during discharge.

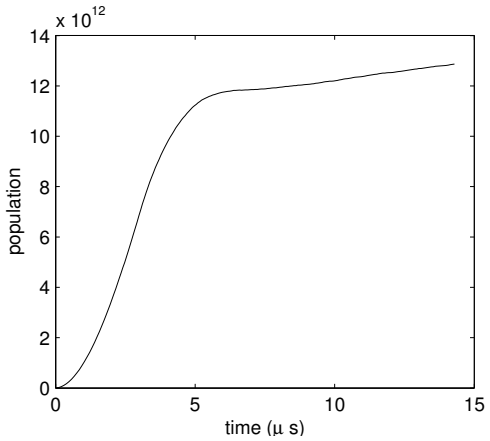

Figure 8: Net Electron population.

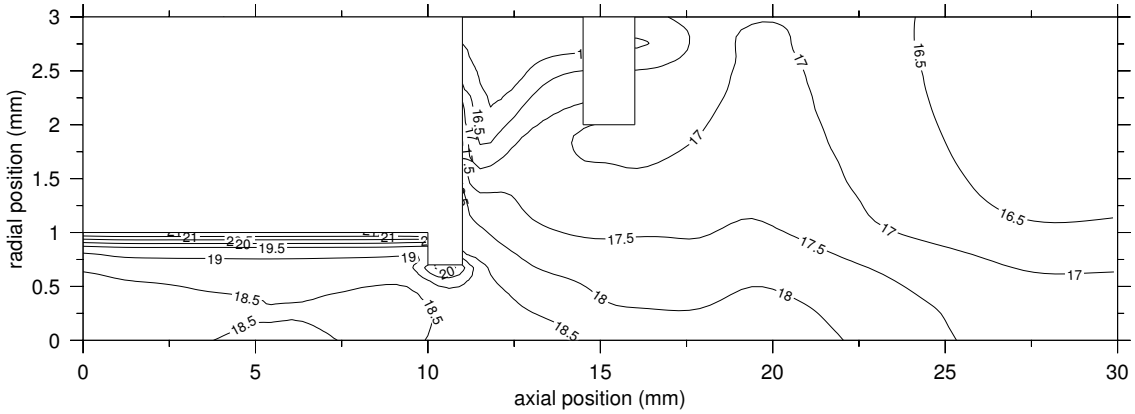

Figure 9: Contours of electron density (labels of 10^x m^{-3})

This has been found to provide a passive, non-invasive upstream condition for the plasma. Other techniques that were tried such as removal of the plasma and/or a 0 V Dirichlet boundary to the field equation were found to interfere to a great extent with the development and evolution of the discharge.

Plasma discharge - initial results

The electron time step is required to be very small; this is the outstanding problem associated with the use of fully particle based models (versus hybrid models). Due to such a constraint, the results presented here do not represent a fully developed discharge, but rather a transient state. The initial breakdown in the keeper region, followed by movement of the plasma upstream into the insert region is observed. This is associated with the formation of a partially ionized plasma from the neutral gas. Results now presented represent the state of the discharge after 14 μs. Figure 8 shows the absolute electron population contained in the simulation domain; this is a good indicator of the initial state of convergence of particle based codes. Clearly, the heavy particle dynamics cannot have come into equilibrium, but these results still demonstrate several interesting phenomena. Figures 9 and 10 show electron and ion densities respectively. Figure 11 shows the plasma potential, note that for this discharge (0.81 A total current *emitted from the cathode*), the charged particle densities are still comparatively low. Figure 12 shows electron energy contours. This final figure clearly shows the initial region where electrons have energy greater than the first ionization energy of Xenon - in the keeper hill 13 to 17 mm downstream.

Electrons emitted from the cathode form a thin sheath near the insert. Electrons that manage to escape past the tip rapidly gain energy. The potential hill generated by the keeper (fig. 7) accelerates the electrons to above the first ionization energy of Xe (12.12eV [16]). This effect is even more pronounced before any plasma has formed: prior to around 3 μs into the simulation, ions are only present on the potential hill. In fact, the majority of new ionization occuring at the time these data were recorded is near the axis beneath the keeper (in figure 10, within the 10^{17} contour). Since the plasma density is not yet great enough to form ionizing reactions within the cathode sheaths, the discharge is increasing in intensity purely due to continued ionization in the keeper region.

As has been mentioned, ions are created at the summit of the keeper potential hill. More than half of the ions initially accelerate and leave the simulation downstream. Some, however, move toward the cathode and

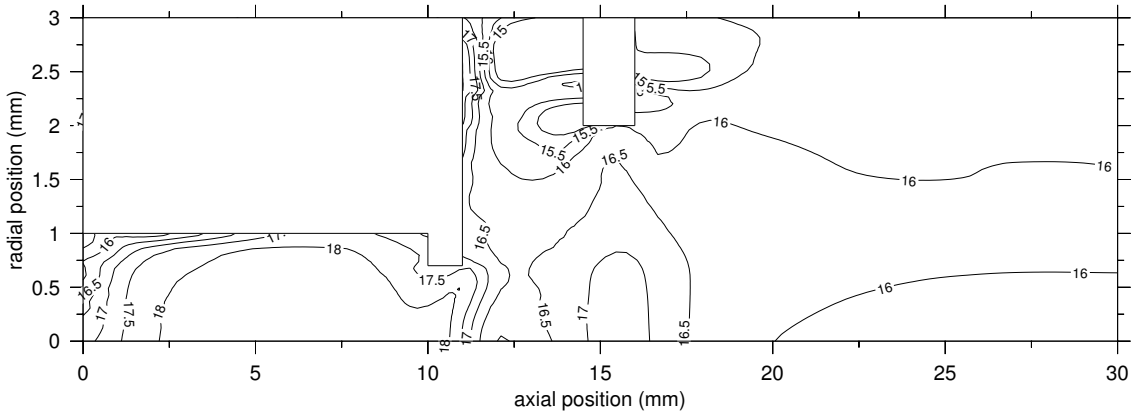

Figure 10: Contours of ion density (labels of 10^x m^{-3})

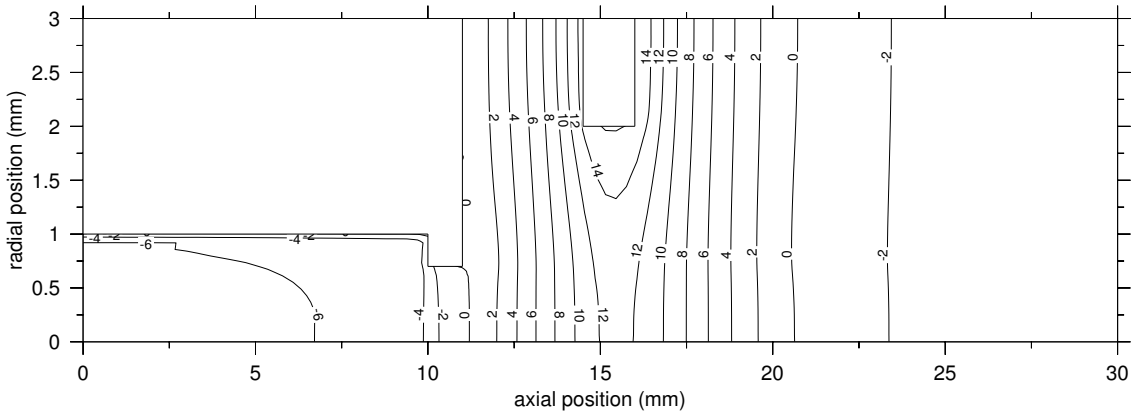

Figure 11: Contours of plasma potential (V).

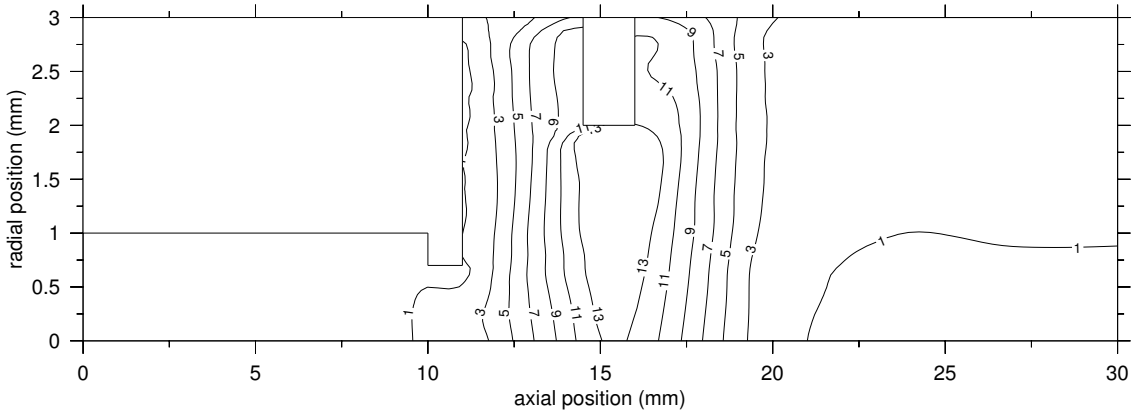

Figure 12: Contours of electron energy (eV).

are observed entering after around 3 μs. This effect causes a choking of the neutral flow in the upstream direction. In fact, the neutral mass flux out of the simulation is seen to drop below 1 mgs^{-1}. This drop in mass flow rate is as a result of two phenomena. First, a small fraction of the neutrals become ions (the ion mass flux out of the simulation is of the order of 10^{-8} mgs^{-1} and rising rapidly). Secondly, the neutral gas in the throat (tip) is bombarded by high energy ions: the neutral stream velocity in the throat at this point is negative and the temperatue raised higher than the cathode (thousands of K). Some gas, as a result of collisions with the high energy ions falling into the cathode, is temporarily being repelled upstream. While this phenomena is transient – eventually the in-flux must equal the out-flux – it is physically realistic and has been observed experimentally. Clearly, the neutral gas is interacting with the plasma in several important ways. Another example of such interaction is on the upstream boundary. Here, the flux of fresh (cold) neutral gas serves to quench the plasma somewhat, resulting in lower ion densities (fig. 10). Within the cathode, the ions form a sheath adjacent to the insert with width of around 1/8 the insert radius. While it is interesting to observe the discharge in this transient state, the heavy particle dynamics clearly need to run on for much longer. It is anticipated, based on experimental observations[17] that a simulation running for at least 200 μ s will be required.

5 Summary and Conclusions

The nature of the neutral gas flow in the hollow cathode geometry has been demonstrated. It has been shown that the cathode behaves like a choked nozzle. The degree of rarefaction that results from the gas expansion through two consecutive normal shock has been demonstrated. This justifies the need to used particle methods. The neutral flow provides a starting condition for the examination of the plasma behavior. An initial characterization of the plasma discharge inside the hollow cathode has been presented. Although much additional work remains, the general structure and behavior of the plasma has been demonstrated. The nature of the initial breakdown has been modeled computationally, also further analysis is required to verify and understand the phenomena shown.

Further improvements to the neutral model concern the modeling of gas interaction with walls. An examination of the effect of incomplete thermal accommodation and hence increased evidence of high Kn slip flow may yield some additional gas dynamic observations. Solution of a heat flow equation within the cathode and keeper would provide a more realistic understanding of both the gas heating in the upstream section and the anticipated keeper cooling in the rarefied supersonic region. Extensions to the understanding of the plasma discharge clearly involve applying further optimizations and/or compute time to the problem, as current results represent a non-equilibrium snapshot of events. The primary requirement, as is generally the case for PIC codes, is optimizations in the field solver speed, as this represents the greatest fraction of run time. A low bandwidth fully parallel spectral (Fourier transform) solver has been developed and shows promise in this area. A trick that has been used for similar PIC simulations – multiplication of the electron mass of 10^3 – can also be tried[4]. In terms of physical reality, extensions involve improvements to the surface interaction physics: secondary electron emission and other complex cathode surface reactions.

References

[1] F. T. Crawford and S. Gabriel, "Modeling small hollow cathode discharges for ion microthrusters," *AIAA 2002–2101*, May 2002.

[2] P. Gessini, S. Gabriel, and D. Fearn, "The hollow cathode as a micro-ion thruster," *Proceedings of the 27th International Electric Propulsion Conference, Pasadena, California*, Oct. 2001.

[3] M. Jugroot and J. Harvey, "Particle simulation of the main chamber of a Kaufmann-type ion thruster," *Proceedings of the 3rd International Conference on Spacecraft Propulsion, ESA SP–465, Cannes, France*, 2000.

[4] Y. Okawa and H. Takegahara, "IEPC-99–146: Particle simulation of ion beam extraction phenomena in an ion thruster," in *Proceedings of the 26th International Electric Propulsion Conference, Kitakyushu, Japan*, pp. 805–812, JSASS, Oct. 1999.

[5] R. I. Samantha Roy, D. E. Hastings, and S. Taylor, "Three-dimensional plasma Particle-In-Cell calculations of ion thruster backflow contamination," *Journal of Computational Physics*, vol. 128, no. 1, pp. 6–18, 1996.

[6] I. D. Boyd, D. Van Guilder, and X. Liu, "Monte Carlo simulation of neutral Xenon flows in electric propulsion devices," *Journal of Propulsion and Power*, vol. 14, pp. 1009–1015, Nov. 1998.

[7] G. M. Sandonato, J. J. Barroso, and A. Montes, "Magnetic confinement studies for performance enhancement of a 5cm ion thruster," *IEEE Transactions on Plasma Science*, vol. 24, pp. 1319–1329, Dec. 1996.

[8] R. Wirz, J. Escobedo, P. Sheehan, J. Polk, C. Marrese, and J. Mueller, "Development and testing of a 3cm electron bombardment micro-ion thruster," *Proceedings of the 27th International Electric Propulsion Conference, Pasadena, California*, Oct. 2001.

[9] M. W. Crofton, "The feasibility of hollow cathode ion thrusters: A preliminary characterization," *AIAA paper 2000–5354*, July 2000.

[10] M. J. Patterson and J. E. Foster, "Hollow cathode micro-thruster performance," *Proceedings of the 27th International Electric Propulsion Conference, Pasadena, California*, Oct. 2001.

[11] K. Nanbu, "Probability theory of electron-molecule, ion-molecule, molecule-molecule, and Couloub collisions for particle modeling of materials processing plasmas and gases," *IEEE Transactions on Plasma Science*, vol. 28, pp. 971–990, June 2000.

[12] G. Bird, *Molecular Gas Dynamics and the Direct Simulation of Gas Flows*. No. 42 in Oxford Engineering Science Series, Oxford University Press, 1994.

[13] V. V. Serikov, S. Kawamoto, and K. Nanbu, "Particle-In-Cell plus direct simulation Monte Carlo (PIC-DSMC) approach for self-consistent plasma-gas simulations," *IEEE Transactions on Plasma Science*, vol. 27, pp. 1389–1398, Oct. 1999.

[14] C. K. Birdsall and A. B. Langdon, *Plasma Physics via Computer Simulation*. Institute of Physics Publishing, 1991.

[15] D. Murray, O. Tutty, and S. Gabriel, "Numerical modelling of the gas flow in an ion thruster hollow cathode," in *Proceedings of the 2nd European Spacecraft Propulsion Conference*, pp. 217–233, Aug. 1997.

[16] J. Pack, R. Voshall, A. Phelps, and K. L.E., "Longitudinal electron diffusion coefficients in gases: Noble gases," *Journal of Applied Physics*, vol. 71, pp. 5363–5371, June 1992.

[17] I. Ahmed Rudwan and S. Gabriel, "Investigation of the discharge characteristics of the T6 hollow cathode operating on several inert gases and a Kr/Xe mixture," *11th International Congress on Plasma Physics, Sydney, Australia*, July 2002.